Title
The Ozone–Climate Penalty: Past, Present, and Future

Journal
Environmental Science and Technology, 47(24)

ISSN
0013-936X

Authors
Rasmussen, DJ
Hu, Jianlin
Mahmud, Abdullah
et al.

Publication Date
2013-12-17

DOI
10.1021/es403446m

Peer reviewed

Published in final edited form as:
Environ Sci Technol. 2013 December 17; 47(24): 14258–14266. doi:10.1021/es403446m.

The ozone-climate penalty: past, present, and future

D.J. Rasmussen[†,¶], **Jianlin Hu**[†], **Abdullah Mahmud**[‡,¶], and **Michael J. Kleeman**[*,†]
Department of Civil and Environmental Engineering, University of California Davis, Davis CA 95616, and Department of Civil and Environmental Engineering, Portland State University, Portland OR 97207

Abstract

Climate change is expected to increase global mean temperatures leading to higher tropospheric ozone (O_3) concentrations in already polluted regions, potentially eroding the benefits of expensive emission controls. The magnitude of the "O_3-climate penalty" has generally decreased over the past three decades which makes future predictions for climate impacts on air quality uncertain. Researchers attribute historical reductions in the O_3-climate penalty to reductions in NO_x emissions, but have so far not extended this theory into a quantitative prediction for future effects. Here we show that a three-dimensional air quality model can be used to map the behavior of the O_3-climate penalty under varying NO_x and VOC emissions in both NO_x-limited and NO_x-saturated conditions in Central and Southern California, respectively. Simulations suggest that the planned emissions control program for O_3 precursors will not diminish the O_3-climate penalty to zero as some observational studies might imply. The results further demonstrate that in a NO_x-limited air basin, NO_x control strategies alone are sufficient to both decrease the O_3-climate penalty and mitigate O_3 pollution, while in a NO_x-saturated air basin, a modified emissions control plan that carefully chooses reductions in both NO_x and VOC emissions may be necessary to eliminate the O_3-climate penalty while simultaneously reducing base case O_3 concentrations to desired levels. Additional modeling is needed to determine the behavior of the O_3-climate penalty as NO_x and VOC emissions evolve in other regions.

Introduction

Surface ozone (O_3) is a secondary pollutant produced by the photochemical oxidation of CO and/or volatile organic compounds (VOCs) by hydroxyl radical ($^{\bullet}HO$) in the presence of oxides of nitrogen ($NO_x \equiv NO_2 + NO$). Model perturbation studies have identified temperature as the most important weather variable affecting surface O_3 concentrations in polluted regions (1–5). These findings have been validated against observations on multiple time scales that have shown strong correlations between temperature and O_3 concentrations

[*]To whom correspondence should be addressed: mjkleeman@ucdavis.edu, Phone: +1 (530) 752-8386. Fax: +1 (530) 752-7872.
[†]Department of Civil and Environmental Engineering, University of California Davis, Davis CA 95616
[‡]Department of Civil and Environmental Engineering, Portland State University, Portland OR 97207
[¶]Now at California Air Resources Board, Sacramento, CA 95814

Supporting Information Available
Supplemental figures showing the location of the ozone receptors used in this study and model results for each air basin showing the spatial distribution of the ozone-climate penalty are available online.
This material is available free of charge via the Internet at http://pubs.acs.org/.

in excess of about 60 ppb (6–8). California is home to seven of the top ten most heavily O_3 polluted metropolitan areas in the United States [1], despite the dramatic reductions of NO_x and VOC precursor emissions over the past three decades (3–6, 9–11). A warming climate is expected to exacerbate surface O_3 in California's two major air basins: the South Coast Air Basin (SoCAB) and the San Joaquin Valley (SJV). Median surface temperatures during the O_3 season over Western North America, including the SoCAB and SJV, are projected to warm between +1 to +5 K by the end of the 21st century (12). These temperature increases may counter the benefits from pollution control strategies used in an effort to meet established air quality standards, resulting in a "climate penalty" (13, 14).

In this study, the sensitivity of O_3 to temperature and NO_x and VOC emissions is calculated in both NO_x-saturated and NO_x-limited conditions with a reactive chemical transport model during two historical severe weekday pollution episodes in California: the SoCAB during September 7–9, 1993 (NO_x-saturated) (15, 16) and the SJV during July 25–27, 2005 (NO_x-limited). Historical episodes are used for the base case analysis to enable the study of O_3-temperature relationships over a period spanning the past two decades to future conditions over which NO_x and VOC emissions have evolved. The results in this study are presented as an O_3 isopleth diagram that simultaneously describes the maximum concentration (ppb) and sensitivity to temperature (ppb K^{-1}) of surface O_3 under specified NO_x and VOC emissions (17). This map of O_3-temperature relationships is compared to historical trends for validation and then projected forward to predict climate impacts on future O_3 pollution.

The O_3-climate penalty

Varying definitions of the O_3-climate penalty have been presented in the literature. Wu et al. consider the climate penalty to represent either the additional decreases in NO_x emissions to counter any climate driven increase in O_3 (assuming NO_x is the limiting precursor) or the reduced benefits of emissions controls due to the increase in O_3 due to a warmer climate (14). Bloomer et al. calculate the "ozone-climate penalty factor", the slope of the best fit line between long-term observational measurements of O_3 and temperature (18). Other studies utilizing air quality models quantified the change in O_3 due to a prescribed temperature perturbation, but did not refer to this sensitivity as a "climate penalty" (3, 4, 6). Here, we employ the temperature perturbation approach and refer to the direct increase in O_3 concentrations due to increasing temperatures (ppb K^{-1}) as the "O_3-climate penalty" or "climate penalty". Previous work has shown the past and present climate penalty to be highly varied in space and time due to differing chemical and meteorological environments that influence O_3 formation (3, 4, 6, 8, 18). The aggregate effects that make up this relationship (the total derivative, $d[O_3]/dT$) are thought to include at least three components:

$$\frac{d[O_3]}{dT}=\frac{\partial[O_3]}{\partial[stagnation]}*\frac{d[stagnation]}{dT}+\frac{\partial[O_3]}{\partial[reaction]}*\frac{d[reaction]}{dT}+\frac{\partial[O_3]}{\partial[BVOC]}*\frac{d[BVOC]}{dT}+\ldots$$

[1]American Lung Association, State of the Air Report. 2013; http://www.stateoftheair.org/2012/city-rankings/most-polluted-cities.html

The first term accounts for the association of warm temperatures with stagnant air masses that facilitate the accumulation of O_3 precursor species (19); the second term accounts for the increase in chemical reaction rates for different species, including the thermal decomposition of alkyl nitrates (AN) and subspecies peroxyacetylnitrate (PAN), reservoirs for both NO_x and HO_x at low temperatures (7); the third term accounts for temperature dependent variations in biogenic emissions of VOCs (BVOCs), which act as a significant source of precursors for O_3 formation under high-NO_x conditions and tend to increase with temperature for many species (20, 21). The ellipsis indicates several additional contributing temperature-dependent processes of varying sign that may not be dominant under the assumptions of the current study, including wildfires in the western US (22) and humidity in the Mid Atlantic (23) (see Table 1 in ref. 24 for a comprehensive list). Model perturbation studies resolve the climate penalty partial derivatives, while observations ascertain the total derivative. Extrapolation of present day O_3-temperature relationships to future climate to estimate changes in O_3 air quality assumes invariable emission rates and ignores complex chemistry-climate interactions (13, 24, 25).

Historical trend in O_3-climate penalty in California

Fig. 1 shows the trend in average daily NO_x and VOC emissions in the SoCAB and the SJV, along with the corresponding decadal trend in the climate penalty from previous model perturbation and observational studies. The climate penalty is strongly correlated with NO_x and VOC emissions in both the SoCAB and the SJV. From 1980 to 2010, average daily emissions of NO_x and VOCs in the SoCAB decreased roughly two and fourfold, respectively; in the SJV NO_x and VOC emissions decreased by a factor of one-and-a-half and three, respectively (26). The dramatic decrease in these emissions reflects the success of California's statewide emission control programs. Over this same period, the mean value of climate penalty in the SoCAB decreased from +8.0 ppb K^{-1} in the 1980s to a present-day value of +2.7 ppb K^{-1}, while the climate penalty in the SJV decreased from a value of +2.8 ppb K^{-1} in the 1980s to a current value of +1.8 ppb K^{-1} (3, 4, 6, 8, 18). Similar NO_x-climate penalty trends have been observed elsewhere. In the eastern U.S., a 43% reduction in power plant NO_x emissions between 1995 and 2002 was shown to correspond to a 1.0 ppb K^{-1} decrease in the O_3-climate penalty (18, 27). Over the next decade, emissions of NO_x and VOCs are expected to continue to decrease in both the SoCAB and the SJV raising the question: will the O_3-climate penalty effectively diminish to zero, or does a particular emissions strategy exist that minimizes the O_3-climate penalty?

Methods

Model description

The UC-Davis-California Institute of Technology (UCD-CIT) air quality model is a 3D Eulerian, photochemical model that simulates reactive chemical transport in the atmosphere and predicts the concentration of both primary and secondary pollutants in the gas and particle phase. Relevant chemical reactions are modeled with the SAPRC11 mechanism (28). A coupled online UV radiative extinction calculation accounts for the scattering and absorption of light due to high airborne particulate matter concentrations to give a more

accurate representation of actinic flux. A more thorough description of the UCD-CIT airshed model and its evolution has been presented previously (16, 29–32).

Due to variations in the physical characteristics of each air basin, different model configurations were used to simulate each pollution episode. The horizontal resolution used in the SoCAB simulations was 5 km × 5 km. The vertical domain was divided into 5 levels (thickness of 38.5, 115.5, 154, 363, and 429m), extending from the surface to 1.1 km above ground. This relatively shallow model depth is only appropriate in well-defined air basins, such as the SoCAB, where pollutants have a residence time of only a few days. The horizontal resolution in the SJV simulations was 8 km × 8 km, and the vertical distance from the surface to 5 km above ground was divided into 16 levels (the surface to 1.1 km above ground for the SJV simulations is comprised of 11 levels). In the SoCAB, hourly 2D and 3D meteorological fields (temperature, absolute humidity, wind speed and direction, and solar intensity) were interpolated from observations using the method described by refs. 33 and 34, while the SJV simulations used hourly meteorological fields generated over California at 4 km × 4 km horizontal resolution with the Weather Research and Forecasting model (WRF) v3.4 (35), driven by the North American Regional Reanalysis (NARR) (36). Four dimensional data assimilation (FDDA) is further used to nudge WRF model estimates closer to observed conditions. The WRF meteorological fields were averaged to 8 km × 8 km to reduce model simulation times. Previous studies have shown these configurations to well reproduce measured pollutant concentrations (16, 37).

The base case emission inventories for the SoCAB and SJV episodes were obtained from the South Coast Air Quality Management District (SCAQMD) and the California Air Resources Board (ARB) and are summarized in refs. 38 and 39, respectively. Boundary conditions at the western edge of each modeling domain were based on measured background concentrations of pollutants that are transported to California (40, 41) and remained constant while emission perturbations were applied. Biogenic emissions were generated at 8 km × 8 km spatial resolution using the Biogenic Emission Inventory Geographic Information System (BEIGIS) model (42). A year 2000 land-use pattern generated by the Moderate-resolution Imaging Spectroradiometer (MODIS) satellite is used to determine vegetation types and leaf area indices. Hourly averaged surface air temperature and shortwave radiation from the meteorology is used to calculate emissions of isoprene, monoterpenes, and 2-methyl-3-buten-2-ol (MBO) (20, 21). In the SJV, livestock feed VOC emissions were estimated using the method described by ref. 43 and are mapped to the spatial distribution of livestock ammonia emissions. Predicted O_3 concentrations for both pollution episodes in this study had performance statistics that met U.S. Environmental Protection Agency (EPA) guidance for air quality models (44).

Calculating the O_3-climate penalty

To generate an O_3 isopleth diagram, the episode base case emissions of NO_x and anthropogenic VOCs were uniformly scaled up (more emissions) or down (less emissions) to represent a hypothetical range of pollution control strategies in each air basin. Here, the air quality model explicitly simulates 121 and 64 NO_x and VOC emissions scenarios in the SoCAB and SJV, respectively. These simulations are then repeated after applying a

temperature perturbation for a total of 370 model runs. In this study, a spatially uniform temperature perturbation was applied to every hour during both multi-day pollution events to calculate a value of the climate penalty at each NO_x and VOC emissions point. This technique explores the O_3-climate penalty under base case conditions to better understand important relationships between emissions and climate. Further work would be required to account for detailed future emissions trends and projected climate patterns if the effects of these secondary factors on future O_3-climate penalties are of interest.

The O_3-climate penalty was calculated as the difference between the O_3 concentrations predicted with the base case temperature profile and the base case temperature profile plus a −5 K perturbation, divided by the magnitude of the temperature perturbation (ppb K^{-1}). The magnitude of the perturbation is arbitrary and is not intended to reflect a projection of future temperature change. Previous work has shown the O_3-climate penalty is not strongly sensitive to the absolute magnitude of the temperature perturbation used (3). A negative (rather than positive) temperature perturbation was chosen in the present study because maximum daily temperatures from the base case episodes were greater than 40°C and the contributions to $d[O_3]/dT$ from PAN decomposition and isoprene emissions have been shown to diminish at temperatures >39°C (8). Not fully accounting for these contributions could lead to an under prediction of the base case O_3 sensitivity to temperature. The negative perturbation produces temperatures that are more in line with historical temperature ranges and therefore yields values of $\partial[O_3]/\partial T$ that are more directly comparable to $d[O_3]/dT$ calculated from long-term measurements of O_3 and temperature (e.g. (6, 8, 18, 45)).

In this study, the temperature perturbation affects chemical kinetic reaction rates and biogenic emissions of isoprene, monoterpenes, and MBO (20, 21). The temperature perturbation does not alter the evaporation of anthropogenic VOCs (46) or the emission rate of soil NO_x and is uncoupled from temperature dependent meteorological variables such as mixed layer depth, solar insolation, wind speed and wind direction; model perturbation studies have shown that mixed layer depth has weak positive and negative effects on O_3 concentrations in polluted regions (1, 3). Temperature driven changes to atmospheric circulation are not considered and could be important in defining the exact meteorological characteristics of peak O_3 episodes. Vegetation and land use data remain constant.

The Clausius-Clapeyron relation predicts exponential increases in the atmosphere's capacity to hold water vapor with increasing temperature. Increases in water vapor can lead to greater HO_x production which may affect O_3 formation differently depending on the region and the atmospheric conditions (1, 2, 4, 47). The temperature perturbations applied in the current study were coupled with different assumptions about humidity for each air basin depending on their geographical features. The majority of the SoCAB is close to the Pacific Ocean where an unlimited water reservoir maintains an approximately constant relative humidity (RH) with increasing temperature. The RH was therefore held constant in the SoCAB when temperature was perturbed. In the SJV, the supply of moisture is limited, and it was therefore assumed that absolute humidity would remain constant with increasing temperature, leading to a decrease in RH. Additional SJV modeling simulations that assumed constant RH resulted in O_3-climate penalty values nearly identical to those that fixed absolute humidity.

Results and discussion

Decreases in NO_x and VOC emissions and the O_3-climate penalty response

Isopleths of 8-h. average O_3 (10:00–18:00 LDT) (ppb) and O_3-climate penalty (ppb K^{-1}) for NO_x and VOC emissions rates relative to conditions on September 8–9, 1993 are shown in Fig. 2 at Downtown Los Angeles, Azusa, Claremont, and Anaheim in the SoCAB. Ozone isopleth diagrams generated for Visalia, Fresno, Hanford, and Bakersfield in the SJV for conditions on July 27, 2005 are shown in Fig. 3. The SoCAB is an urban environment that is NO_x-saturated during weekdays (48), while both the SJV and the eastern U.S. are predominantly NO_x-limited at all times (49). Each isopleth shows the modeled base case O_3 concentration under a particular set of NO_x and VOC emissions rates with the same meteorology. In these simulations, NO_x is emitted from both soil and anthropogenic sources and VOC is emitted from anthropogenic and natural sources. For both air basins, NO_x and only anthropogenic VOC emissions are scaled. The scaling factors are the fraction of NO_x and VOC emissions relative to the base years. The base year for the SJV episode is 2005 and the base year for the SoCAB episode is 1993. Base years have a scaling factor of 1. The range of scaling factors was chosen to capture the range of both historical and projected emissions.

The colors overlaid on each O_3 isopleth diagram in Figs. 2 and 3 show the magnitude of O_3-climate penalty (ppb K^{-1}). The maximum in the O_3-climate penalty occurs at a NO_x emission level slightly greater than that which produces the maximum O_3 under the base case temperature simulation and at the highest VOC emission rates. This is coincident with the "O_3 isopleth ridge", or the line of maximum O_3 formation. The minimum in O_3-climate penalty occurs in conditions that are appreciably NO_x-saturated. The simulations here suggest that when NO_x emissions are much greater than VOC emissions, the O_3-climate penalty may become strongly negative (i.e. a climate "benefit") at Downtown LA and Anaheim (−0.1 to −0.4 ppb K^{-1}) (O_3 decreases with increasing temperature), suggestive of O_3 titration by NO from further NO_x-saturation that results from the thermal decomposition of PAN at hotter temperatures (7).

The historical and projected trend (1990—2020) in average daily anthropogenic NO_x and VOC emissions rates, relative to the respective base case inventory, is drawn on each isopleth diagram as black (historical) and grey (projected) dots connected by a dashed black line, taken together to constitute an emissions "trajectory". Receptors in each air basin are assumed to experience an equivalent rate of NO_x and VOC emissions reductions. The O_3 values along the NO_x-VOC emissions trajectory are an estimate of the maximum amount of O_3 pollution that could be formed during a severe pollution event with similar meteorology. Substantially NO_x-saturated conditions are not predicted by the emissions trajectory at any of the SoCAB or SJV receptors over the next decade (Figs. 2 and 3).

In both air basins, the O_3 isopleth diagrams suggest that NO_x and VOC emission reductions between 1990 and 2010 have been effective at abating O_3 during weekday severe pollution events, especially in eastern LA and the SJV, confirming previous findings (10, 26). Reductions in O_3 in the SoCAB were accomplished through reductions in emissions of both NO_x and VOCs. Fig. 2 shows that reductions in NO_x emissions alone over this 20-year

period would have increased O_3 concentrations in the SoCAB. Little change in O_3 is seen at both Anaheim and Downtown LA (Fig. 2a, d) because reductions in NO_x and VOC emissions produce a trajectory that stays within a zone of approximately constant O_3. In the SJV, reductions in O_3 have primarily occurred through reductions in NO_x emissions.

Over the next decade, the ARB projects that NO_x and VOC emissions will continue to decrease in both air basins, with NO_x emissions declining more rapidly. Projections for the SoCAB indicate that this emissions trajectory may not be optimal, with slight increases in O_3 concentrations (+20–30 ppb under the meteorological conditions studied). This result is consistent with findings from other investigators; Fujita et al. find that reductions in NO_x emissions without concurrent VOC emission reductions over the next decade will cause O_3 to increase in central portions of the SoCAB during weekdays (9). No such effect is predicted for the SJV in the present study; the O_3 isopleths for the SJV predict continued decreases in O_3 over the next decade under meteorological conditions conducive to O_3 formation (Fig. 3).

The historical and projected trend in the O_3-climate penalty can be inferred from the NO_x-VOC emission trajectory on the isopleths (Figs. 2 and 3). Both NO_x and VOC emissions appear to play a role in determining the O_3-climate penalty in the SoCAB, contrary to previous findings that suggest NO_x emissions are the primary explanatory variable in the observed decreasing trend in the O_3-climate penalty (18). Reducing NO_x emissions, primarily emitted as nitric oxide (NO), in a NO_x-saturated environment can exacerbate O_3 pollution by both decreasing O_3 loss by NO titration and increasing the ratio of VOCs to NO_x, favoring peroxy (HO_2) and alkylperoxy (RO_2) formation, both of which propagate the chain reaction mechanism that produces O_3 in the troposphere (50). While NO_x emission controls may be effective at decreasing the O_3-climate penalty in the NO_x-limited eastern U.S. and SJV (18, 49), the results of the current study suggest that further decreases in VOC emissions over the next decade in the SoCAB (NO_x-saturated) may be beneficial to reducing base case O_3 pollution and may additionally be effective at minimizing the O_3-climate penalty.

Future trend in the O_3-climate penalty and implications

The O_3 isopleth diagrams illustrate climate penalty-emissions relationships at individual receptor sites, but do not readily facilitate an air-basin wide assessment of historical and projected trends in the O_3-climate penalty along the emissions trajectory. To characterize an air-basin wide climate penalty, we use 18 urban receptor sites in the SJV and 26 urban receptor sites in the SoCAB. The location of these receptors are shown in supporting information, Fig. S1, and are analogous to the receptor sites that are used by ref. 8. Fig. 4 shows the modeled historical (1985—2010) and projected (2015—2020) trend in O_3-climate penalty (ppb K^{-1}) at these receptor sites in the SoCAB (left) and the SJV (right). Modeled results are presented as box-and-whisker plots (25th, median, and 75th percentiles) where the whiskers are the mean (not shown) ± the standard deviation. Values outside of the whiskers are plotted as crosses. Historical values of the O_3-climate penalty from the literature (as both air basin averages and at individual receptors) are drawn as solid black symbols. Values

given by ref. 8 are decadal air basin averages constructed from long-term measurements and likely capture the full O_3-temperature relationship.

The observed trend of the O_3-climate penalty from all literature sources are generally well reproduced by the air quality model using the meteorology from severe pollution events that are characterized by very hot surface temperatures (r^2=0.98 in the SoCAB; r^2=0.69 in the SJV). The median model prediction is systematically lower than the measured climate penalty from ref. 8 by, at most, 0.8 ppb K^{-1} in the SoCAB over the past three decades, but is reproduced to within ±0.3 ppb K^{-1} in the SJV from the 1990s to the 2000s. In the SJV, site-by-site differences in the O_3-climate penalty are more pronounced (> 1 ppb K^{-1}), including between the current and past model perturbation studies (3, 5) and may reflect differing assumptions therein. Differences between modeled and observed values may reflect emissions sector changes (i.e. changes to VOC reactivity (51)) during the past three decades that are not captured using the uniform emissions scaling approach employed here, or other contributions that are not captured with the simple temperature perturbation approach that only affects kinetic rate constants, biogenic emission rates, and water vapor concentrations in a representative episode. For example, calculation of the O_3-climate penalty from long-term modeled O_3 and surface temperature may yield different sensitivities than those derived from a single severe pollution event as some contributing components of the full O_3-temperature relationship may be driven by intra-seasonal weather patterns and events. The choice of biogenic emissions models and chemical mechanisms may also influence the predicted climate penalty. The sensitivity of the results to these modeling options should be investigated in future work.

The range of climate penalties at receptors in the SoCAB in 1985 varies by about a factor of 30, +0.7 ppb K^{-1} to +26.2 ppb K^{-1}, a substantially wider range of variability compared to the SJV, +0.6 ppb K^{-1} to +3.9 ppb K^{-1}. Receptors east of Los Angeles that are adjacent to the San Gabriel Mountains (a large source of biogenic VOCs) have the largest climate penalties through out the simulation period (1985—2020)(Fig. S2a). These sites are likely sensitive to increased biogenic VOC emissions through rises in temperature. The central and coastal receptors in the SoCAB consistently have the lowest climate penalty, as they may be saturated with fresh NO emissions that titrate O_3. While the future median O_3-climate penalty is projected to decrease steadily in both air basins, some receptors in the SoCAB near the San Gabriel Mountains (e.g. Azusa and Claremont, Fig. 2b–c) are expected to experience a rise in the climate penalty due to the strengthening sensitivity of O_3 to strong biogenic emissions in a region where NO_x decreases much more rapidly than VOC emissions. The 2020 median O_3-climate penalty is projected to be +0.8 ppb K^{-1} in the SoCAB (basin-wide range of −0.8 ppb K^{-1} to +11.8 ppb K^{-1}) and +0.9 ppb K^{-1} in the SJV (basin-wide range of 0.0 ppb K^{-1} to +1.5 ppb K^{-1}), suggesting under the projected emissions pathway, increases in temperature due to climate change may continue to have deleterious effects on O_3 control programs. Although average daily NO_x and VOC emissions are projected to decrease 37% and 12%, respectively, over the next decade in the SoCAB (26), potential concomitant anthropogenic VOC emissions reductions may be beneficial to reduce both base case O_3 and to further diminish the O_3-climate penalty.

In NO_x limited regions such as the SJV and the eastern US, continued decreases in NO_x emissions are anticipated and may continue to lower the O_3-climate penalty. The exact O_3-temperature relationship at other locations should be evaluated for a representative episode of interest (peak or average) using an appropriate reference year (historical or present-day). Future studies should also account for climate-driven changes to atmospheric circulation, changes in land use, choice of boundary conditions that reflect changes to long range transport of pollutants, and scaling individual emissions sectors to accurately reflect emission control targets.

Supplementary Material

Refer to Web version on PubMed Central for supplementary material.

Acknowledgments

Research reported in this publication was partially supported by the National Institutes of Health under Award Number ES020237. The content is solely the responsibility of the authors and does not necessarily represent the official views of the National Institutes of Health. We thank M. Hixson for data processing tools to prepare the model inputs. We acknowledge three anonymous reviewers, C. Anastasio, C. Cappa (UC-Davis), J. Chen and A. Kaduwela (CARB) for all providing comments on earlier versions of the manuscript.

References

1. Aw J, Kleeman MJ. Evaluating the first-order effect of intraannual temperature variability on urban air pollution. J Geophys Res-Atmos. 2003; 108
2. Dawson JP, Adams PJ, Pandis SN. Sensitivity of ozone to summertime climate in the eastern USA: A modeling case study. Atmos Environ. 2007; 41:1494–1511.
3. Kleeman MJ. A preliminary assessment of the sensitivity of air quality in California to global change. Climatic Change. 2008; 87:S273–S292.
4. Millstein DE, Harley RA. Impact of climate change on photochemical air pollution in Southern California. Atmos Chem Phys. 2009; 9:3745–3754.
5. Steiner AL, Tonse S, Cohen RC, Goldstein AH, Harley RA. Influence of future climate and emissions on regional air quality in California. J Geophys Res -Atmos. 2006; 111:D18303.
6. Mahmud A, Tyree M, Cayan D, Motallebi N, Kleeman MJ. Statistical down-scaling of climate change impacts on ozone concentrations in California. J Geophys Res -Atmos. 2008; 113:D21103.
7. Sillman S, Samson FJ. Impact of temperature on oxidant photochemistry in urban, polluted rural and remote environments. J Geophys Res -Atmos. 1995; 100:11497–11508.
8. Steiner AL, Davis AJ, Sillman S, Owen RC, Michalak AM, Fiore AM. Observed suppression of ozone formation at extremely high temperatures due to chemical and biophysical feedbacks. Proc Natl Acad Sci USA. 2010; 107:19685–19690. [PubMed: 21041679]
9. Fujita EM, Campbell DE, Stockwell WR, Lawson DR. Past and future ozone trends in California's South Coast Air Basin: Reconciliation of ambient measurements with past and projected emission inventories. J Air Waste Manage Assoc. 2013; 63:54–69.
10. Parrish DD, Singh HB, Molina L, Madronich S. Air quality progress in North American megacities: A review. Atmos Environ. 2011; 45:7015–7025.
11. Warneke C, de Gouw JA, Holloway JS, Peischl J, Ryerson TB, Atlas E, Blake D, Trainer M, Parrish DD. Multiyear trends in volatile organic compounds in Los Angeles, California: Five decades of decreasing emissions. J Geophys Res-Atmos. 2012; 117
12. Chistensen, J., et al. Climate Change 2013: The Physical Science Basis. In: Fyfe, J.; Kwon, W-T.; Trenberth, K.; Wratt, D., editors. Contribution of Working Group I to the Fifth Assessment Report of the Intergovernmental Panel on Climate Change. Cambridge University Press; Cambridge, United Kingdom and New York, NY, USA: 2014.

13. Jacob DJ, Winner DA. Effect of climate change on air quality. Atmos Environ. 2009; 43:51–63.
14. Wu S, Mickley LJ, Leibensperger EM, Jacob DJ, Rind D, Streets DG. Effects of 2000–2050 global change on ozone air quality in the United States. J Geophys Res -Atmos. 2008; 113:D06302.
15. Fraser MP, Kleeman MJ, Schauer JJ, Cass GR. Modeling the atmospheric concentrations of individual gas-phase and particle-phase organic compounds. Environ Sci Technol. 2000; 34:1302–1312.
16. Ying Q, Fraser MP, Griffin RJ, Chen J, Kleeman MJ. Verification of a source-oriented externally mixed air quality model during a severe photochemical smog episode. Atmos Environ. 2007; 41:1521–1538.
17. Sillman S. The relation between ozone, NO_x and hydrocarbons in urban and polluted rural environments. Atmos Environ. 1999; 33:1821–1845.
18. Bloomer BJ, Stehr JW, Piety CA, Salawitch RJ, Dickerson RR. Observed relationships of ozone air pollution with temperature and emissions. Geophys Res Lett. 2009; 36:L09803.
19. Jacob DJ, Logan JA, Yevich RM, Gardner GM, Spivakovsky CM, Wofsy SC, Munger JW, Sillman S, Prather MJ, Rodgers MO, Westberg H, Zimmerman PR. Simulation of summertime ozone over North America. J Geophys Res -Atmos. 1993; 98:14797–14816.
20. Guenther AB, Zimmerman PR, Harley PC, Monson RK, Fall R. Isoprene and monoterpene emission rate variability - model evaluations and sensitivity analyses. J Geophys Res -Atmos. 1993; 98:12609–12617.
21. Harley P, Fridd-Stroud V, Greenberg J, Guenther A, Vasconcellos P. Emission of 2-methyl-3-buten-2-ol by pines: A potentially large natural source of reactive carbon to the atmosphere. J Geophys Res -Atmos. 1998; 103:25479–25486.
22. Pfister GG, Wiedinmyer C, Emmons LK. Impacts of the fall 2007 California wildfires on surface ozone: Integrating local observations with global model simulations. Geophys Res Lett. 2008; 35
23. Camalier L, Cox W, Dolwick P. The effects of meteorology on ozone in urban areas and their use in assessing ozone trends. Atmos Environ. 2007; 41:7127–7137.
24. Fiore AM, et al. Global air quality and climate. Chem Soc Rev. 2012; 41:6663–6683. [PubMed: 22868337]
25. Weaver CP, et al. A preliminary synthesis of modeled climate change impacts on U.S. regional ozone concentrations. B Am Meteorol. 2009; 90:1843–1863.
26. Cox, P.; Delao, A.; Komorniczak, A.; Weller, A. The California Almanac of Emissions and Air Quality. 2009. 2009.
27. Kim SW, Heckel A, McKeen SA, Frost GJ, Hsie EY, Trainer MK, Richter A, Burrows JP, Peckham SE, Grell GA. Satellite-observed US power plant NO_x emission reductions and their impact on air quality. Geophys Res Lett. 2006; 33
28. Carter WP, Heo G. Development of revised *SAPRC* aromatics mechanisms. Atmos Environ. 2013; 77:404–414.
29. Kleeman M, Cass G. A 3D Eulerian source-oriented model for an externally mixed aerosol. Environ Sci Technol. 2001; 35:4834–48. [PubMed: 11775160]
30. Kleeman MJ, Cass GR, Eldering A. Modeling the airborne particle complex as a source-oriented external mixture. J Geophys Res -Atmos. 1997; 102:21355–21372.
31. McRae GJ, Goodin WR, Seinfeld JH. Development of a second-generation mathematical model for Urban air pollution-I. Model formulation. Atmos Environ. 1982; 16:679–696.
32. Mysliwiec MJ, Kleeman MJ. Source apportionment of secondary airborne particulate matter in a polluted atmosphere. Environ Sci Technol. 2002; 36:5376–5384. [PubMed: 12521164]
33. Goodin WR, McRae GJ, Seinfeld JH. An objective analysis technique for constructing three-dimensional urban-scale wind fields. J Appl Meteorol. 1980; 19:98–108.
34. Goodin WR, McRae GJ, Seinfeld JH. A comparison of interpolation methods for sparse data: Application to wind and concentration fields. J Appl Meteorol. 1979; 18:761–771.
35. Skamarock WC, Klemp JB. A time-split nonhydrostatic atmospheric model for weather research and forecasting applications. J Comput Phys. 2008; 227:3465–3485.
36. Mesinger F, et al. North American regional reanalysis. B Am Meteorol. 2006; 87:343.

37. Hu J, Howard CJ, Mitloehner F, Green PG, Kleeman MJ. Mobile source and livestock feed contributions to regional ozone formation in Central California. Environ Sci Technol. 2012; 46:2781–2789. [PubMed: 22304388]
38. Griffin RJ, Dabdub D, Kleeman MJ, Fraser MP, Cass GR, Seinfeld JH. Secondary organic aerosol - 3. Urban/Regional scale model of size- and composition-resolved aerosols. J Geophys Res-Atmos. 2002; 107
39. Ying Q, Lu J, Kaduwela A, Kleeman MJ. Modeling air quality during the California Regional PM10/PM2.5 Air Quality Study (CPRAQS) using the UCD/CIT source oriented air quality model - part II. Regional source apportionment of primary airborne particulate matter. Atmos Environ. 2008; 42:8967–8978.
40. Fraser MP, Grosjean D, Grosjean E, Rasmussen RA, Cass GR. Air quality model evaluation data for organics. - 1. Bulk chemical composition and gas/particle distribution factors. Environ Sci Technol. 1996; 30:1731–1743.
41. Liang J, Horowitz LW, Jacob DJ, Wang Y, Fiore AM, Logan JA, Gardner GM, Munger JW. Seasonal budgets of reactive nitrogen species and ozone over the United States, and export fluxes to the global atmosphere. J Geophys Res -Atmos. 1998; 103:13435–13450.
42. Scott KI, Benjamin MT. Development of a biogenic volatile organic compounds emission inventory for the SCOS97-NARSTO domain. Atmos Environ. 2003; 37(Supplement 2):39–49.
43. Howard CJ, Kumar A, Malkina I, Mitloehner F, Green PG, Flocchini RG, Kleeman MJ. Reactive organic gas emissions from livestock feed contribute significantly to ozone production in central California. Environ Sci Technol. 2010; 44:2309–14. [PubMed: 20192169]
44. United States EPA. Guidance on the Use of Models and Other Analyses for Demonstrating Attainment of Air Quality Goals for Ozone, PM2.5, and Regional Haze. 2007.
45. Rasmussen DJ, Fiore AM, Naik V, Horowitz LW, McGinnis SJ, Schultz MG. Surface ozone-temperature relationships in the eastern US: A monthly climatology for evaluating chemistry-climate models. Atmos Environ. 2012; 47:142–153.
46. Rubin JI, Kean AJ, Harley RA, Millet DB, Goldstein AH. Temperature dependence of volatile organic compound evaporative emissions from motor vehicles. J Geophys Res-Atmos. 2006; 111
47. Baertsch-Ritter N, Keller J, Dommen J, Prevot ASH. Effects of various meteorological conditions and spatial emission resolutions on the ozone concentration and ROG/NO_x limitation in the Milan area (I). Atmos Chem Phys. 2004; 4:423–438.
48. Pollack IB, et al. Airborne and ground-based observations of a weekend effect in ozone, precursors, and oxidation products in the California South Coast Air Basin. J Geophys Res - Atmos. 2012; 117:2156–2202.
49. Duncan BN, Yoshida Y, Olson JR, Sillman S, Martin RV, Lamsal L, Hu Y, Pickering KE, Retscher C, Allen DJ, Crawford JH. Application of OMI observations to a space-based indicator of NO_x and VOC controls on surface ozone formation. Atmos Environ. 2010; 44:2213–2223.
50. Seinfeld, JH.; Pandis, SN. Atmospheric chemistry and physics: from air pollution to climate change. 2. J. Wiley; Hoboken, N.J: 2006. p. xxviiip. 1203
51. Pusede SE, Cohen RC. On the observed response of ozone to NO_x and VOC reactivity reductions in San Joaquin Valley California 1995 to present. Atmos Chem Phys. 2012; 12:8323–8339.

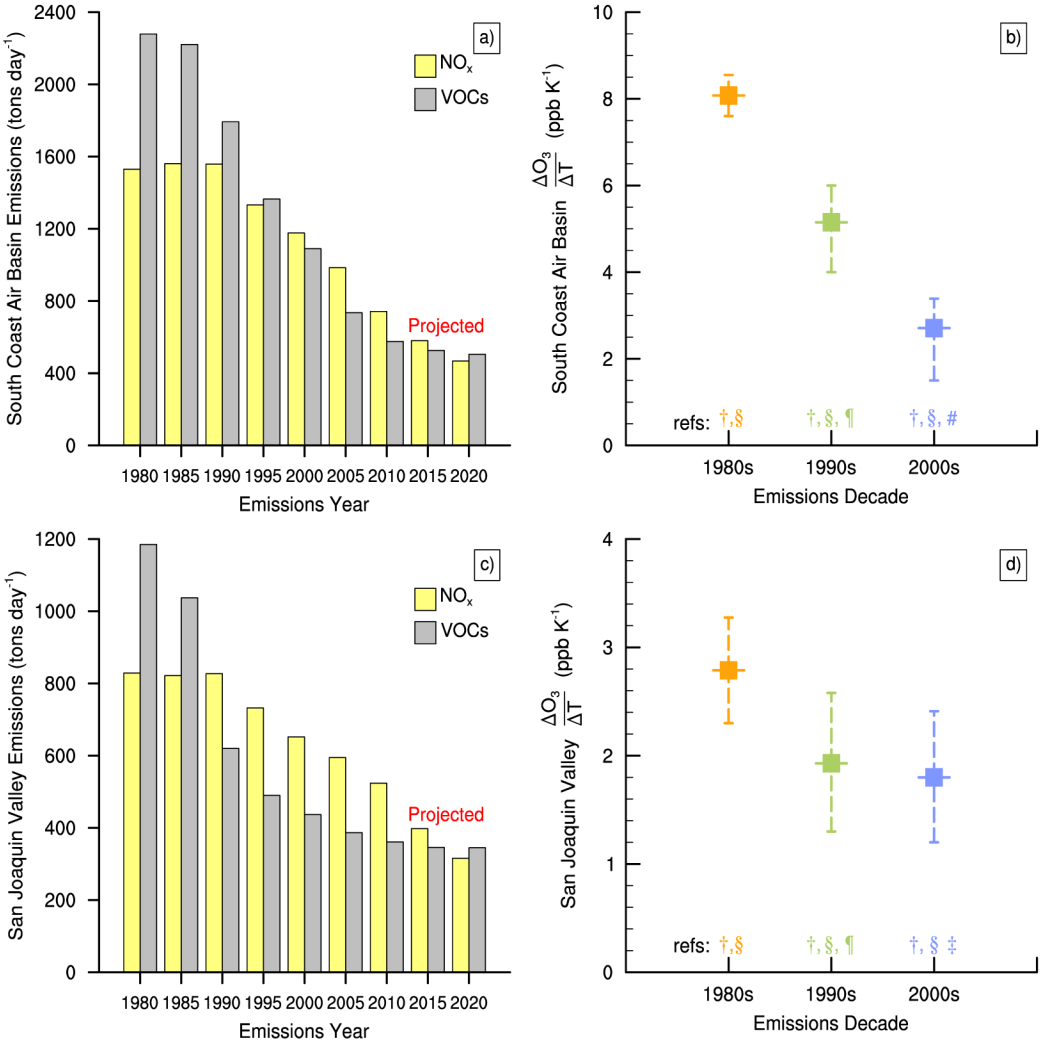

Figure 1.

(a) Historical and projected average daily anthropogenic NO_x (yellow) and VOC (gray) emissions (tons day^{-1}) versus emissions year for the South Coast Air Basin and (b) the observed decadal trend in the O_3-climate penalty for the Southern California Air Basin attributed to emissions changes during the 1980s (orange), the 1990s (green), and the 2000s (blue). Dashed lines give the range of both observed and modeled O_3-climate penalty values in the South Coast Air Basin from the literature; solid squares are the mean O_3-climate penalty calculated from values given in the literature. Symbols beneath each range correspond to literature references: † is Mahmud et al., 2008 (statistical downscaling based on measured trends), § is Steiner et al., 2010 (observations), ¶ is Kleeman, 2008 (model perturbation), # is Millstein and Harley, 2009, (model perturbation), and ‡ is Steiner et al., 2006 (model perturbation); (c) as for (a) but for the San Joaquin Valley; (d) as for (b) but for the San Joaquin Valley.

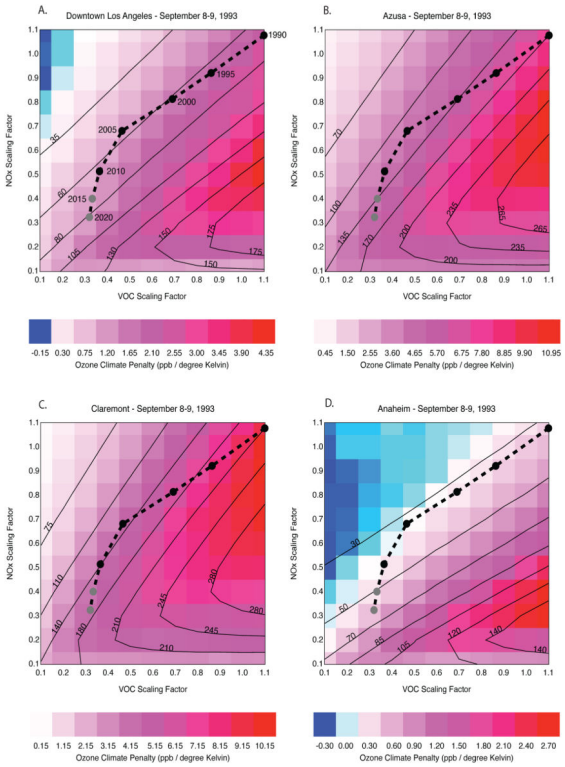

Figure 2.

Isopleths of 8 hr. average O_3 (ppb)(solid black lines) and O_3-climate penalty (ppb K^{-1}) (colors) generated from a −5 K temperature perturbation for (a) Downtown Los Angeles, (b) Azusa, (c) Claremont, and (d) Anaheim. All calculations are for the conditions on September 8–9, 1993. Estimated anthropogenic emissions trend relative to the 1993 base year is shown as a dashed black line. A different color scale is used for each panel.

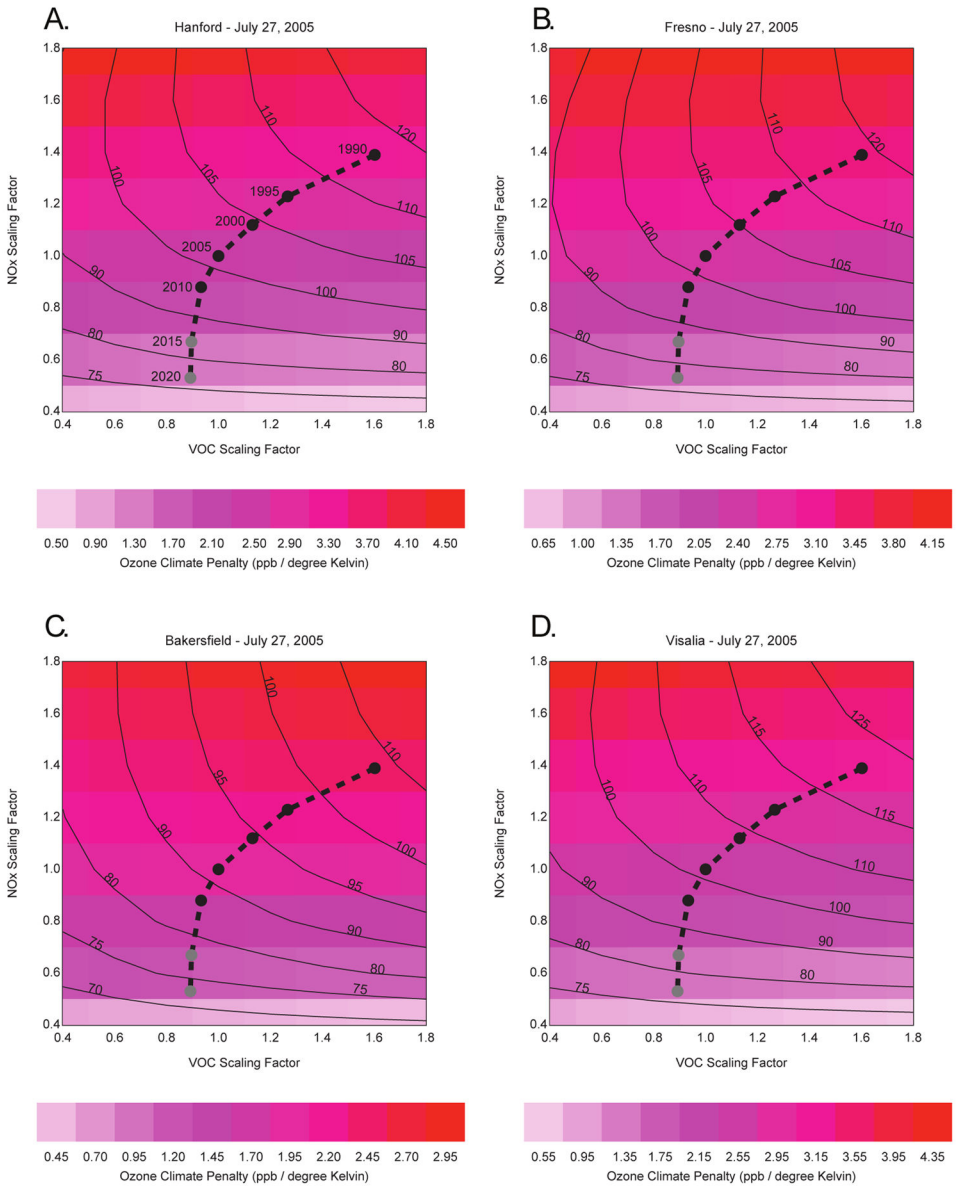

Figure 3.

Isopleths of 8 hr. average O_3 (ppb)(solid black lines) and O_3-climate penalty (ppb K^{-1}) (colors) generated from a −5 K temperature perturbation for (a) Hanford, (b) Fresno, (c) Bakersfield, and (d) Visalia. All calculations are for the conditions on July 27, 2005. Estimated anthropogenic emissions trend relative to the 2005 base year is shown as a dashed black line. A different color scale is used for each panel.

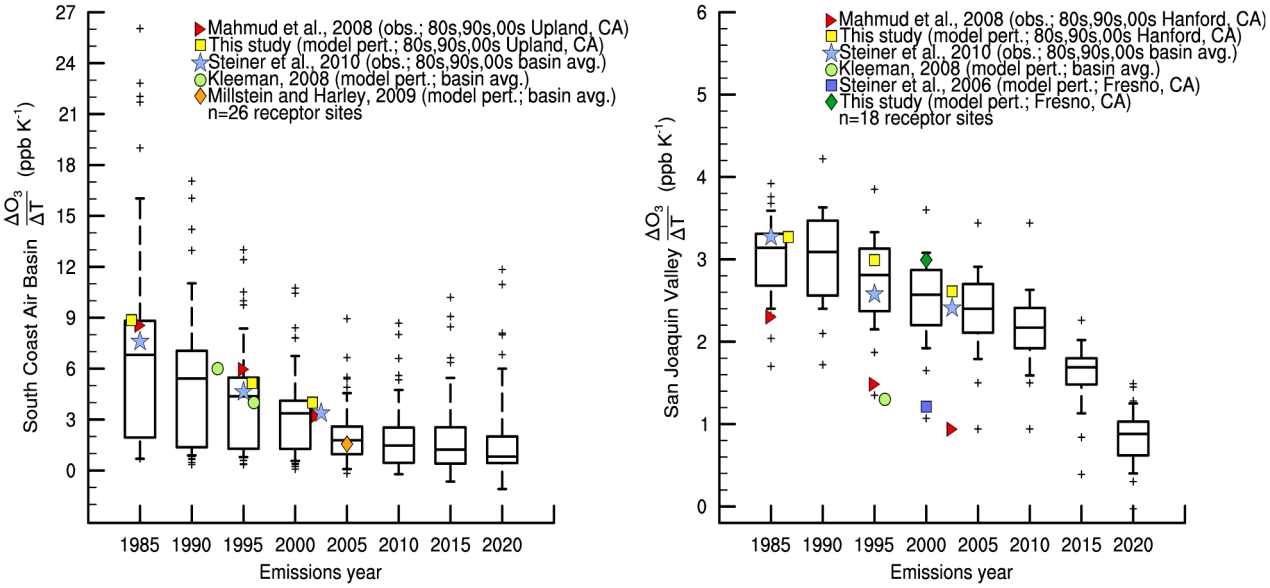

Figure 4.

Historical (colored markers) and modeled O_3-climate penalty (ppb K^{-1}) for emissions years from 1985 to 2020 for the South Coast Air Basin (SoCAB) (left) and the San Joaquin Valley Air Basin (SJV) (right). The box-and-whisker plots (mean minus the standard deviation, 25th, 50th, 75th, and mean plus the standard deviation) give statistics of the modeled O_3-climate penalty at 26 urban receptors in the South Coast Air Basin and at 18 urban receptors in the San Joaquin Valley (*see* supporting information, Fig. S1). Values greater or less than the mean ± the standard deviation are shown as crosses. All modeled calculations are for the conditions on September 8–9, 1993 (SoCAB) and July 27, 2005 (SJV).